

Molecular Dynamics Simulation of Bauschinger Effect in Cu Nanowire with Different Crystallographic Orientation

Sefa KAZANÇ¹, Canan AKSU CANBAY^{2*}

¹ Mathematics and Science Education, Faculty of Education, Fırat University, Elazığ, Türkiye

² Department of Physics, Faculty of Science, Fırat University, 23119 Elazığ, TÜRKİYE

¹ skazanc@firat.edu.tr, ^{2*} caksu@firat.edu.tr

(Geliş/Received: 11/09/2023;

Kabul/Accepted: 27/03/2024)

Abstract: In this study, the Bauschinger Effect (BE) resulting from tension-compression deformation applied to nanowires obtained by placing Cu atoms in $\langle 100 \rangle$, $\langle 110 \rangle$ and $\langle 111 \rangle$ highly symmetric crystallographic directions was investigated using the Molecular Dynamics (MD) simulation method. The forces between atoms were determined from the gradient of the Embedded Atom Method (EAM) potential function, which includes many-body interactions. It was determined that there is an asymmetry between the stress-strain curves obtained as a result of the tension and compression deformation process applied to the model system. From this asymmetry, it was determined that the yield stress obtained in the drawing process for nanowire with $\langle 100 \rangle$ crystallographic orientation was greater than the yield strain obtained as a result of the compression process. In contrast, the opposite was found for nanowires with crystallographic orientation $\langle 110 \rangle$ and $\langle 111 \rangle$. In addition, after the yield strain value is exceeded as a result of the drawing process applied to the model nanowire system, compression deformation process was applied at different pre-strain values. The existence of the Bauschinger Effect (BE), which is expressed as the yield strength value as a result of forward loading corresponding to the tension operation, is smaller than the yield value obtained as a result of the compression process in which the loading is removed, was determined. To clarify the effect of BE on Cu nanowires with different crystallographic orientations, Bauschinger Stress parameter (BSP) and Bauschinger Parameter (BP) values were calculated.

Key words: Nanowire, Bauschinger effect, crystallographic orientation, mechanical properties, molecular dynamics.

Farklı Kristalografik Yönetime Sahip Cu Nano Telindeki Bauschinger Etkisinin Moleküler Dinamik Benzetimi

Öz: Bu çalışmada, Cu atomlarının $\langle 100 \rangle$, $\langle 110 \rangle$ ve $\langle 111 \rangle$ yüksek simetrik kristalografik doğrultulara yerleştirilmesiyle elde edilen nano tellere uygulanan çekme-sıkıştırma deformasyonu sonucu oluşan Bauschinger Etkisi (BE) Moleküler Dinamik (MD) benzetim yöntemi kullanılarak incelendi. Çok cisim etkileşimlerini içeren Gömülmüş Atom Metodu (GAM) potansiyel fonksiyonunun gradientinden atomlar arasındaki kuvvetler belirlendi. Model sisteme uygulanan çekme ve sıkıştırma deformasyon işlemi sonucu elde edilen zor-zorlanma eğrileri arasında bir asimetri olduğu belirlendi. Bu asimetriden $\langle 100 \rangle$ kristalografik yönetime sahip nano tel için çekme işleminde elde edilen akma geriliminin sıkıştırma işlemi sonucu elde edilen akma geriliminden daha büyük olduğu belirlendi. Buna karşılık $\langle 110 \rangle$ ve $\langle 111 \rangle$ kristalografik yönetime sahip nano teller için tam tersi bir durum tespit edildi. Ayrıca model nano tel sistemine uygulanan çekme işlemi sonucu akma gerinim değeri aşıldıktan sonra farklı ön-gerinim değerlerinde sıkıştırma deformasyon işlemi uygulandı. Çekme işlemine karşılık gelen ileri yüklemeye sonucu akma dayanımı değerinin yüklenmenin kaldırıldığı sıkıştırma işlemi sonucu elde edilen akma değerinden küçük olması olarak ifade edilen Bauschinger Etkisi (BE)'nin varlığı belirlendi. BE'nin farklı kristalografik yönetime sahip Cu nano telleri üzerindeki etkisini açıklığa kavuşturmak için Bauschinger Stress parametresi (BSP) ve Bauschinger Parametresi (BP) değerleri hesaplandı.

Anahtar kelimeler: Nano tel, Bauschinger etkisi, kristalografik yönelim, mekanik özellikler, moleküler dinamik.

1. Introduction

Nanowires are of great technological importance due to their potential applications in nanoscale electrical, optical, thermal and mechanical systems. These nanowires allow for the construction of nanoelectromechanical systems with unprecedented functions [1-4]. However, in addition to their physical and chemical properties, since these devices are exposed to external forces and deformation where they are used, it is extremely important to know their mechanical properties. Therefore, it is necessary to know the deformation mechanisms of nanowires under complex stress conditions. Since nanowires have a large surface area to volume ratio compared to bulk materials, their structure and properties are quite different from bulk materials.

The different crystallographic orientations of nanowires significantly affect their mechanical properties such as Young's modulus, yield stress, yield strain plastic deformation mechanism. Diano et al. [5] observed an

* Corresponding author: caksu@firat.edu.tr. ORCID Number of authors: ¹0000-0002-8896-8571, ²0000-0002-5151-4576

unsymmetrical yield stress in the Au nanowire for $\langle 100 \rangle$, and $\langle 110 \rangle$, orientations due to surface-acting internal forces and different shear systems during tension-compression. Park et al. [6,7] studied the effects of stress deformation for fcc nanowires with different crystallographic orientations.

It is known that during the tension-compression deformation process applied to the sample, the symmetry in the stress-strain relationship is preserved only within the elastic region boundaries. Bauschinger observed in 1886 that this symmetry breaks down when the yield stress of the material is exceeded. If a material is plastically deformed in one direction, plastic yielding in the reverse loading direction occurs at a lower stress than in the forward loading direction. In general, during plastic deformation, dislocations stack up against obstacles of different kinds. This decrease in yield stress in the reverse loading direction is known as the Bauschinger effect (BE) [8, 9]. BE; It is observed in many single and polycrystalline metallic materials, including Al [10], Cu [11], Nb [12,], steel [13]. However, its amount varies from metal to metal, depending on its microstructural properties. Many industrial applications are affected by BE, such as metal forming processes, flattening of sheets and bars [14-16]. This effect minimizes the accumulation of defects and significantly affects the service life and performance of metallic components during cyclic loading processes such as fatigue [17], wear [18,19] by reducing stress concentrations. Although many studies have been conducted to investigate the origin of BE, the number of models and theories developed is very few [20].

Cu element exhibits anisotropic properties depending on the crystal orientation and its mechanical properties such as yield strength and modulus of elasticity vary considerably [21,22]. However, Cu is widely used in many nano/micro electromechanical systems in circuit construction [23].

Many studies have been carried out to experimentally determine the mechanical properties of nanowires [24-26]. However, atomistic simulation methods, especially MD simulations, produce very realistic results in this area [27,28]. Today, MD simulations are widely and effectively used in materials science research with the latest developments in computer technology. Researchers have carried out extensive experiments and atomistic simulation studies to understand the deformation behavior of fcc, bcc metallic nanowires [29-32]. Compared to experimental measurements, simulation studies provide more structural detail during deformation, allowing us to examine the mechanism from a microscopic perspective. Among many atomic models such as effective medium theory [33], tight binding model [34], Finnis-Sinclair dual function formulation [35], EAM [36] has a solid theoretical basis, density function theory and It is one of the most successful approaches because of its simple analytical expression. To date, EAM has been applied to various systems such as liquids, metals and alloys, semiconductors, ceramics, polymers, nanostructures and composite materials. Structural [37], mechanical [38,39], and thermal properties [40] have been extensively studied in studies.

In this study, the Bauschinger effect in the tension-compression deformation process applied to Cu nanowires with different crystallographic orientations at 10K temperature and $1 \times 10^{10} \text{s}^{-1}$ strain value was investigated by MD simulation method. Large-scale Atomic/Molecular Massively Parallel Simulator (LAMMPS) open source MD simulation program was used for modeling nanowire structures [41]. Plastic deformation of nanowires as a result of tension-compression cycle was determined by CNA analysis method from OVITO [42] program. It was determined that crystallographic orientations had a significant effect on the stress-strain curve of the nanowire system and the BE effect was clearly seen.

1. Simulation Details

The Lagrangian function of the system to be modeled in the MD method is given in (1) below.

$$L_{PR}(\mathbf{r}^N, \dot{\mathbf{r}}^N, \mathbf{h}, \dot{\mathbf{h}}) = \frac{1}{2} \sum_{i=1}^N m_i (\dot{\mathbf{s}}_i^t \mathbf{G} \dot{\mathbf{s}}_i) - \sum_{i=1}^N \sum_{j>i}^N \phi(|\mathbf{h} \mathbf{s}_{ij}|) + \frac{1}{2} M \text{Tr}(\dot{\mathbf{h}}^t \dot{\mathbf{h}}) - P_{ext} V \quad (1)$$

where s_i , \mathbf{h} , \mathbf{G} and P_{ext} parameters define the scaled coordinate, the axes of the calculation cell, the metric tensor and the external pressure, respectively. The equations of motion obtained from this function for the particles and the calculation cell are given in equations (2) and (3), respectively.

$$\ddot{\mathbf{s}}_i = -\frac{1}{m_i} \mathbf{F}_i - \mathbf{G}^{-1} \dot{\mathbf{G}} \dot{\mathbf{s}}_i \quad (2)$$

$$\ddot{\mathbf{h}} = M^{-1} (\Pi - \mathbf{I} P_{ext}) V (\mathbf{h}^t)^{-1} \quad (3)$$

For a system subjected to deformation, the stress is calculated by the microscopic stress tensor as given in equation (4) [43,44].

$$\sigma_{ij} = V^{-1} \left[\sum_{i=1}^N m_i \vartheta_i \vartheta_i - \sum_{i=1}^N \sum_{j>i}^N \frac{F_{ij}}{r_{ij}} \mathbf{r}_i \cdot \mathbf{r}_j \right] \quad (4)$$

An object under the influence of external forces is said to be in a strain state. The state of the stress at any point in the matter is determined by the nine-component stress tensor as in (5).

$$\sigma_{ij} = \begin{pmatrix} \sigma_{11} & \sigma_{12} & \sigma_{13} \\ \sigma_{21} & \sigma_{22} & \sigma_{23} \\ \sigma_{31} & \sigma_{32} & \sigma_{33} \end{pmatrix} \quad (5)$$

The components of the stress tensor σ_{11} , σ_{22} , σ_{33} (which can also be expressed as σ_x , σ_y , σ_z , respectively) are known as the normal components of the stress, and the other components are known as the shear components of the stress. The positive values of the normal components correspond to the tension stress and the negative values to the compression stress. In uniaxial loading applied to the system along the x-axis, only the σ_x component changes. In contrast, the other components are zero [45,46].

EAM is a quasi-experimental potential energy function, which includes many-body interactions and is used to model systems of monoatomic elements and alloys. In EAM, the energy of the system is determined from the energy required to embed an atom in the charge density of other atoms around it. Total energy of the system in EAM is expressed in (6) as;

$$E_{top} = \sum_i^N F_i(\rho_i) + \frac{1}{2} \sum_{i \neq j} \Phi(r_{ij}) \quad (6)$$

The first term in the function, $F_i(\rho_i)$, gives the embedding energy including many-body interactions, and the second term $\Phi(r_{ij})$ gives the two-body interaction [47]. EAM parameters of Cu element can be found in the literature [48].

In this study, nanowire systems were formed by placing Cu atoms at fcc lattice points along the $\langle 100 \rangle$, $\langle 110 \rangle$ and $\langle 111 \rangle$ high symmetry directions. Periodic boundary conditions were applied only along the x-direction. No boundary conditions were applied along the y and z directions. The numerical solution of the equations of motion was carried out with the velocity form of the Verlet algorithm. In order for the pre-tension value of the nanowire to be zero, 5×10^4 MD steps were stabilized using the system NVT canonical ensemble without applying shrinkage for all crystallographic orientations. The strain rate and an integration step were determined as $1 \times 10^{10} \text{ s}^{-1}$ and 1 fs, respectively, in the study. The conjugate gradient algorithm was used to minimize the energy in the initial structure.

Cu nanowires with $\langle 100 \rangle$, $\langle 110 \rangle$ and $\langle 111 \rangle$ orientations used in the study consist of 4647, 4857 and 4903 atoms, respectively. The length of the nanowire was determined as 10.8 nm in the x direction and 2.17 nm in the y and z directions. In the whole study, compression deformation was applied to different oriented Cu nanowires by tension deformation and removal of this deformation at different pre-strain values. Several atomic layers were fixed in the two end regions along the x-direction of the model nanowire system. Dynamic behavior of the remaining atoms in the intermediate region is allowed. In order to comply with the experimental pulling method, one of the fixed ends was kept motionless, while the other end was pulled.

2. Results and Discussion

In this study, the BE of the model systems was investigated by applying tension deformation along the x-axis and compression at certain pre-strain values to nanowires in which Cu atoms were placed at fcc lattice points along the $\langle 100 \rangle$, $\langle 110 \rangle$ and $\langle 111 \rangle$ high symmetry directions. In Figure 1, the initial structures of Cu nanowires with these three different crystal orientations are given. The tension-compression mechanical processing process was applied by keeping the left fixed end of the nanowire motionless, pulling the right fixed end with a strain rate of $1 \times 10^{10} \text{ s}^{-1}$ and removing the tension strain with the same strain rate. Both fixed ends of the nanowire consist of three fixed atomic layers.

In Figure 2(a-c), stress-strain curves obtained as a result of applying the initial tension and compression deformation process separately along the x-axis direction to the initial structures of Cu nanowire systems with crystallographic orientations of $\langle 100 \rangle$, $\langle 110 \rangle$ and $\langle 111 \rangle$ are given. It is noteworthy that crystallographic orientations have a significant effect on the stress-strain curves obtained as a result of the calculations. Cu nanowires show elastic anisotropy as a function of crystal orientation. As seen in Figure 2(a), point A where the strain is 0.11 in the drawing process applied to the $\langle 100 \rangle$ Cu nanowire is the yield point at 7.18 GPa at which plastic deformation begins. Then the voltage drops abruptly to 2.23 GPa at point B. This change in voltage is 4.95

GPa. These changes in tension for $\langle 110 \rangle$ and $\langle 111 \rangle$ nanowires were determined as 3.83 GPa and 8.97 GPa, respectively. This sudden change in the voltage value is known as the nucleation of dislocations within the nanowire system [7,49,50]. Partial dislocations dominated by Shockley partial dislocations slide rapidly along the $\{111\}$ crystal plane, causing a sharp drop in stress [51]. It can be said that the greatest stress variation occurs in the $\langle 111 \rangle$ nanowire and this crystallographic orientation is the optimal arrangement of atoms in the nanowire for nucleation, growth and movement of dislocations. During the compression process applied to the $\langle 100 \rangle$, $\langle 110 \rangle$ and $\langle 111 \rangle$ nanowires, this change in stress was determined as 0.405 GPa, 6.31 GPa and 12.09 GPa, respectively.

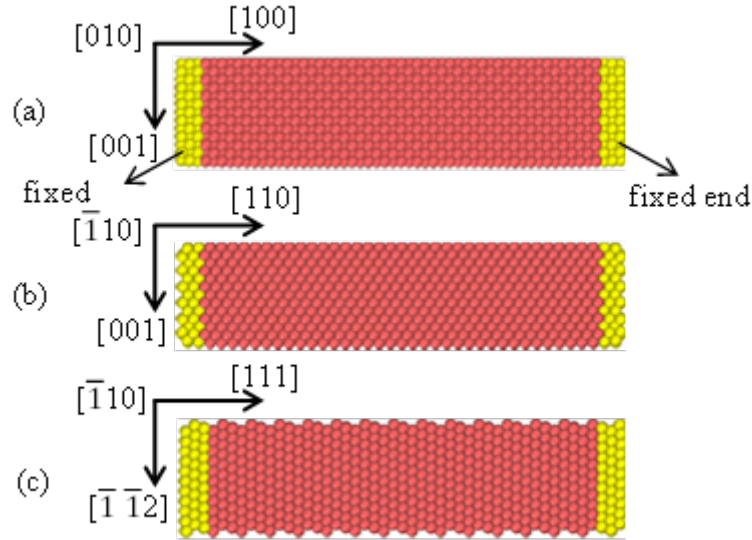


Figure 1. (a) $\langle 100 \rangle$, (b) $\langle 110 \rangle$ and (c) $\langle 111 \rangle$ Initial atomic structures of Cu nanowires. The yellow colored spheres indicate the stationary boundary atoms defined as the fixed end, the red colored spheres the dynamic atoms.

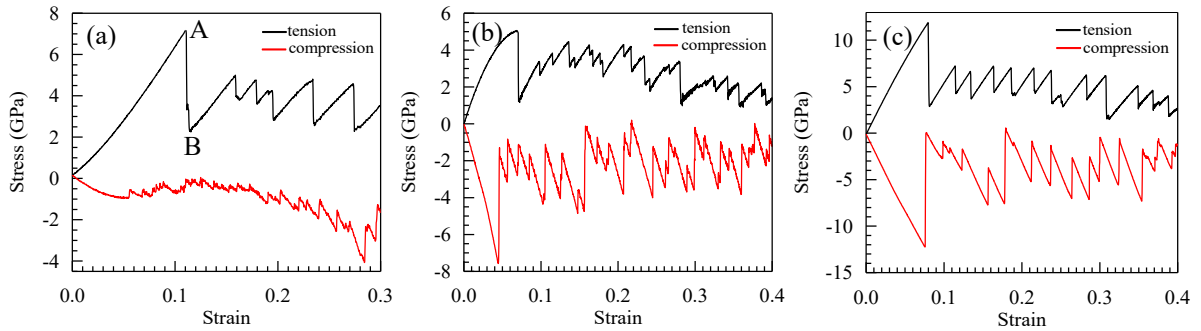


Figure 2. Stress-strain curves for (a) $\langle 100 \rangle$, (b) $\langle 110 \rangle$ and (c) $\langle 111 \rangle$ Cu nanowires obtained as a result of tension-compression deformation.

Figure 3 shows the yield stress (σ_y) in the tension direction, the pre-strain stress (σ_f) in the tension direction and the yield stress (σ_r) in the compression direction in the stress-strain curve obtained as a result of the tension-compression process applied to the nanowire system. Tension and compression deformation in nanowires with all three crystallographic orientations show an asymmetry in mechanical properties related to free surface effects in wires. When the strain reaches 0.056 as a result of the compression applied to the $\langle 100 \rangle$ nanowire system, $\sigma_r = 0.985$ GPa. This value is quite small compared to $\sigma_y = 7.18$ GPa. However, for $\langle 110 \rangle$ and $\langle 111 \rangle$ nanowires, the situation is the opposite ($\sigma_r > \sigma_y$). It is also seen for nanowires with three different crystallographic orientations that the stress-strain curve exhibits a zig-zag change as the strain value continues to increase. It can be said that the reason for this change is due to the growth and spread of nucleated dislocations [52,53]. If both tension and compression yield stresses are equal, the material behaves isotropically. To compare the difference in strength under tension and compressive loads, the tension-compression asymmetry $(\sigma_y - \sigma_r) / \sigma_y$ formula was used [51]. The tension-compression yield strength and calculated tension-compression asymmetry for Cu nanowires with

three different atomic orientations are given in Table 1. It can be clearly seen that the tension compression asymmetry of the $\langle 100 \rangle$ nanowire is more pronounced than that of the $\langle 110 \rangle$ and $\langle 111 \rangle$ nanowires. Tension-compression asymmetry is usually caused by different microscopic mechanisms. However, the different tension-compression asymmetries and BE exhibited by monocrystalline and polycrystalline materials await investigation [51].

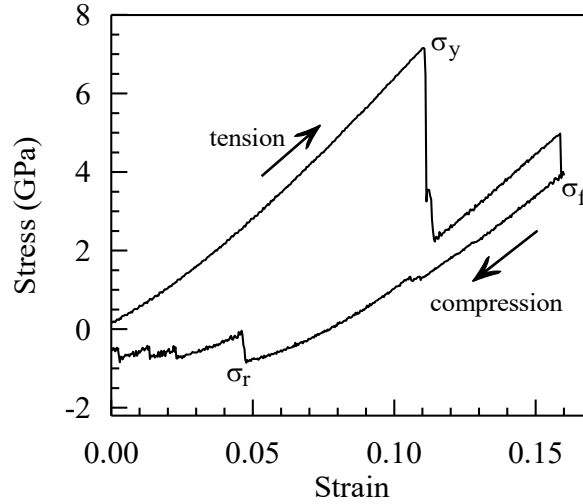


Figure 3. The yield stress in the tension direction (σ_y), the pre-strain stress in the tension direction (σ_f) and the yield stress in the compression direction (σ_r) points in the stress-strain curve obtained as a result of the tension-compression process applied to the Cu nanowire system.

The stress-strain curves obtained as a result of the tension-compression deformation process applied to Cu nanowires with three different crystallographic orientations within elastic limits are given in Figure 4(a-c). First, as seen in Figure 4(a), the $\langle 100 \rangle$ nanowire was subjected to tension processing up to a pre-strain value of 0.08 within the elastic region boundaries. After reaching this strain value, the applied load was removed and compression was performed. The compression yield stress was determined to be 0.985 GPa. This value is the same as the original compression yield stress given in Figure 2(a). The same processes were applied to the $\langle 110 \rangle$ and $\langle 111 \rangle$ nanowires within the elastic region limits, as seen in Figure 4(b-c). The resulting compression yield stresses were found to be the same as the original compression yield stresses. In this case, it was determined that BE was not observed for all three nanowire systems, since the nanowires were not plastically deformed.

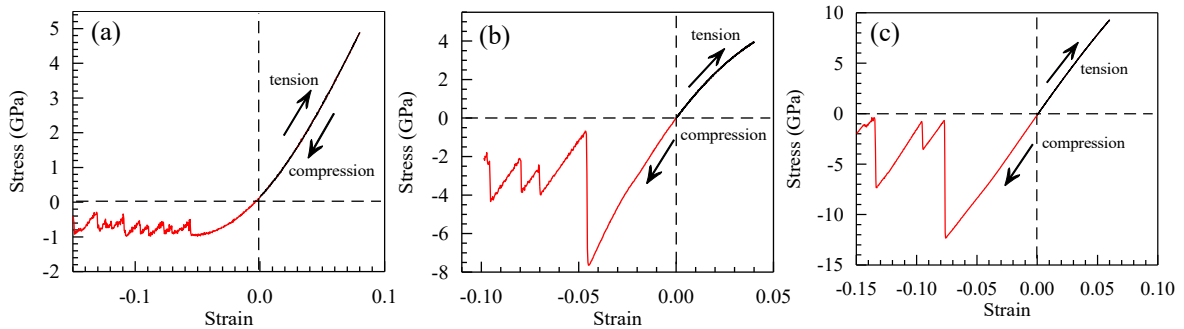
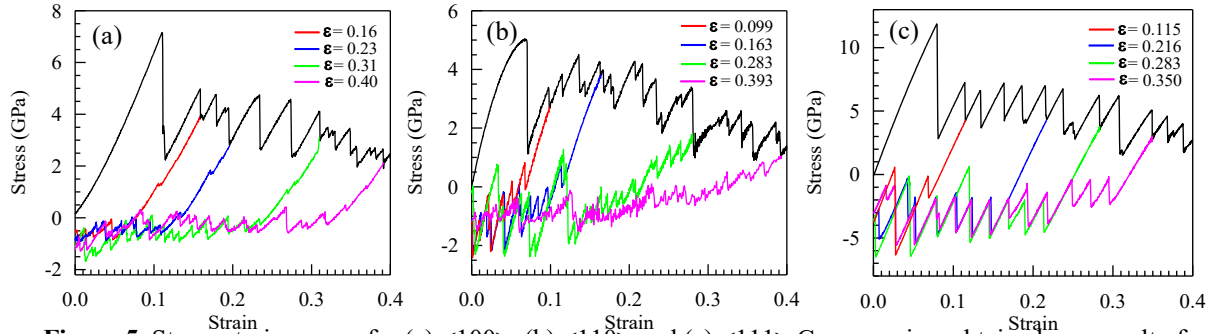


Figure 4. Stress-strain curves for (a) $\langle 100 \rangle$, (b) $\langle 110 \rangle$ and (c) $\langle 111 \rangle$ Cu nanowires obtained as a result of tension and compression deformation within elastic region boundaries.

Table 1. Tension-compression yield stresses and asymmetry of Cu single crystal nanowire.

Orientation	σ_f^t (GPa)	σ_f^c (GPa)	Asymmetry (%)
<100>	7.18	0.98	86.3
<110>	5.06	7.57	-49.6
<111>	11.88	12.29	-3.45

The mechanical response of metals subjected to plastic deformation depends not only on the current stress state, but also on their deformation history. This history can be seen as the difference between tension and compression yield stress in a ductile material [54]. In order to determine the Bauschinger effect depending on the deformation history, as seen in Figure 5(a-c), after the plastic deformation started to occur as a result of the tension loading applied to the nanowires with different crystallographic orientations, reverse loading was performed at different pre-strain values. As seen in Figure 5(a), tension deformation was applied to the <100> nano wire up to the pre-strain values of 0.16, 0.23, 0.31 and 0.40, and after these values, the load was removed and the compression process was performed. The same operations were performed at different pre-strain values in nanowires with other crystallographic orientation, as seen in Figure 5(b-c).

**Figure 5.** Stress-strain curves for (a) <100>, (b) <110> and (c) <111> Cu nanowires obtained as a result of compression deformation for different pre-strain values.

There are two types of mechanisms behind BE. The first mechanism is that during plastic deformation, dislocations accumulate in barriers, producing both long-range and short-range interactions, and dislocation stacks are formed. As a result, back stress develops in the material, which aids the reverse loading dislocation motion. In the second mechanism, when the loading direction is reversed, opposite sign dislocations are produced from the same source. Dislocations attract each other and dislocations disappear. Since stress hardening is related to the dislocation density, decreasing the number of dislocations reduces the strength. The result is that the compression yield strength is smaller than the tension yield strength [55,56]. However, the Bauschinger effect is affected by many factors such as grain boundaries, twinning, interphase boundaries, and second phases [57].

Table 2. BSP and BP values of Cu single crystal nanowire for different crystal orientations and pre-strain values.

Orientation	pre-strain (ϵ)	0.16	0.23	0.31	0.40
<100>	σ_f (GPa)	3.95	3.55	3.10	2.09
	σ_r (GPa)	-0.85	-0.66	-0.52	-0.29
	BSP	0.78	0.81	0.83	0.85
	BP	0.13	0.32	0.47	0.70
ϵ		0.09	0.16	0.28	0.39
<110>	σ_f (GPa)	2.72	3.83	1.80	1.03
	σ_r (GPa)	-0.13	-0.06	0.85	0.35
	BSP	0.95	0.98	0.52	0.66
	BP	0.98	0.99	0.88	0.95
ϵ		0.11	0.21	0.28	0.35
<111>	σ_f (GPa)	4.32	4.31	3.82	3.12
	σ_r (GPa)	-6.35	-4.57	-4.56	-2.38
	BSP	-0.47	-0.06	-0.19	0.23
	BP	0.48	0.63	0.62	0.81

Many different definitions have been used to measure the magnitude of the Bauschinger effect. The Bauschinger effect can be observed qualitatively from stress-strain curves. In order to quantitatively explain the Bauschinger effect for nanoscale simulation studies, Abel (1987) introduced a parameter called the Bauschinger stress parameter (BSP), which is a function of the pre-stress [58,59]. The BSP defines the relative reduction in stress from the forward bias stress to the reverse yield stress. However, Caceres et al. He stated that BSP is a parameter that measures the amount of back stress that particles exert on dislocations in the matrix [60]. where σ_f is the pre-strain stress in the tension direction and σ_r is the yield stress in the compression direction is determined as in eq. (7) below [8];

$$\text{BSP} = \frac{|\sigma_f| - |\sigma_r|}{|\sigma_f|} \quad (7)$$

At the nanoscale, the plastic region of the stress-strain curve appeared to exhibit a saw-like pattern. Since a specific hardening pattern cannot be predicted for the material at this scale, the Bauschinger parameter (BP) is defined in (9) to clarify this effect.

$$\text{BP} = \frac{\sigma_r^o - \sigma_r^c}{\sigma_r^o} \quad (9)$$

In this equation, σ_r^o is the original compression yield stress and σ_r^c is the compression yield stress obtained at different pre-strain values. The definition of the BP parameter indicates that the stronger Bauschinger effect leads to a greater BP value [53]. The calculated BSP and BP values of Cu nanowires with three different crystallographic orientations and different pre-strain for each orientation are given in Table 2. It is seen that the BSP increases as the pre-strain value for the <100> nanowire increases. It is thought that the increase in the pre-strain values at the completion of the tension applied to the sample will cause an increase in the plastic deformation of the material, resulting in a decrease in the difference between σ_f and σ_r values, resulting in a BE effect for this crystallographic orientation. However, it can be said that the <100> nanowire moves away with increasing pre-strain from isotropic strain, which corresponds to the $\sigma_f = \sigma_r$ state and is expressed as the expansion of the yield surface of a material with plastic deformation [54]. In addition, the increase in BP as a result of the increase in the pre-strain value indicates that a stronger BE is formed in the nanowire. In many fcc metals such as Cu, especially in nanoscale crystals, deformation at room temperature is achieved by the formation of deposition defects and the movement of partial dislocations associated with slumping defects [61,62]. Setoodah [53] et al. They found that a larger pre-strain value causes a higher dislocation density in the material and therefore a lower yield strength in the opposite direction. Also, dislocations formed under tension deformation are more likely to slip under compression deformation, resulting in premature yielding. For <110> nanowire, BSP and BP were found to be high at low pre-strains (0.099 and 0.163), and low for high pre-strains (0.283 and 0.393). This corresponds to a greater BE effect in the nanowire at low pre-strain values. With an increase in the amount of forward pre-strain, the number of mobile dislocations may decrease due to more dislocation interaction and possible formation of a more stable dislocation structure [63]. Therefore, with the increase of the amount of pre-strain, the back stress increases up to a certain pre-strain level and then decreases or becomes saturated, depending on the number of mobile dislocations present in the material [64-66]. Compared to nanowires with <100> and <110> crystallographic orientation, it is seen that σ_r value is greater than σ_f value in <111> nanowire, except for the pre-strain value of 0.35. From this, it can be said that the model nanowire structure exhibits reverse BE behavior where the compression yield strength is higher than the tension yield strength. The twin structures formed under compression deformation inhibit the movement of dislocations, causing the compression yield strength to be slightly greater than the tension yield strength, resulting in inverse BE [51]. However, it can be said from the increase in BP value that the increase in pre-strain increases the effect of BE.

3. Conclusion

In this study, the Bauschinger effect, which is the result of uniaxial tension compression deformation applied to Cu nanowires with different crystallographic orientation and modeled with the EAM potential function, was investigated by MD simulation. Crystallographic orientations have a significant effect on the stress-strain curves obtained from the calculations. The existence of tension-compression asymmetry was determined for Cu nanowires with three different atomic orientations. It was determined that the tension-compression asymmetry of the <100> nanowire was more pronounced than that of the <110> and <111> nanowires. BE was clearly seen in the Cu nanowire with different crystallographic orientations. The results of BE are important in nano-scale forming processes of nanomaterials. In single crystal structures, plastic deformation is related to dislocation shift and

twinning. Dislocations formed under tension are more likely to slip under compression, resulting in lower yield stress.

References

- [1] Wang JF, Gudixsen MS, Duan XF, Cui Y, Lieber CM. Highly polarized photoluminescence and photodetection from single indium phosphide nanowires. *Science* 2001; 293: 1455-1457.
- [2] Joyce HJ, Gao Q, Tan HH, Jagadish C, Kim Y, Zou J. et.al. III-V semiconductor nanowires for optoelectronic device applications. *Prog Quant Electron* 2011; 35: 23-75.
- [3] Cui Y, Zhong ZH, Wang DL, Wang WU, Lieber CM. High performance silicon nanowire field effect transistors. *Nano Lett* 2003; 3: 149-152.
- [4] Huang Y, Duan XF, Lieber CM. Nanowires for integrated multicolor nanophotonics. *Small* 2005;1: 142-147.
- [5] Diao J, Gall K, Dunn ML. Yield Strength Asymmetry in Metal Nanowires. *Nano Letters* 2004; 4: 1863-1867.
- [6] Park HS, Zimmerman JA. Modeling inelasticity and failure in gold nanowires. *Physical Review B* 2005; 72: 054106.
- [7] Park HS, Gall K, Zimmerman JA. Deformation of FCC nanowires by twinning and slip. *J. Mech. Phys. Solids* 2006; 54: 1862-1881.
- [8] Mahato JK, De PS, Sarkar A, Kundu A, Chakraborti PC. Effect of deformation mode and grain size on Bauschinger behavior of annealed copper. *International Journal of Fatigue* 2016; 83: 42-52.
- [9] Paul JDH, Hoppe R, Appel F. On the Bauschinger effect in TiAl alloys. *Acta Materialia* 2016; 104: 101-108
- [10] Stoltz RE, Pelloux RM. The Bauschinger effect in precipitation strengthened aluminum alloys. *Metall Trans A* 1976; 7: 1295-1306.
- [11] Pedersen OB, Brown LM, Stobbs WM. The bauschinger effect in copper. *Acta Metall* 1981; 29: 1843-1850.
- [12] Waheed S, Hao R, Bhowmik A, Balint DS, Giuliani F. A unifying scaling for the Bauschinger effect in highly confined thin films: a discrete dislocation plasticity study. *Model Simulat Mater Sci Eng* 2017; 25: 54003.
- [13] Han K, Van Tyne CJ, Levy BS. Effect of strain and strain rate on the bauschinger effect response of three different steels. *Metall Mater Trans A* 2005; 36: 2379-2384.
- [14] Gui HL, Li Q, Huang QX. The influence of Bauschinger effect in straightening process. *Math. Probl. Eng* 2015; 2015: 1-5.
- [15] Chun BK, Kim HY, Lee JK. Modeling the Bauschinger effect for sheet metals, part II: applications. *Int. J. Plast.* 2002; 18: 597-616.
- [16] Chun BK, Jinn JT, Lee JK. Modeling the Bauschinger effect for sheet metals, part I: theory, *Int. J. Plast.* 2002; 18: 571-595.
- [17] Srivatsan TS, Al-Hajri M, Troxell JD. The tensile deformation, cyclic fatigue and final fracture behavior of dispersion strengthened copper. *Mech. Mater.* 2004; 36: 99-116.
- [18] Tang CY, Li DY, Wen GW. Bauschinger's effect in wear of materials. *Tribol. Lett.* 2010; 41: 569-572.
- [19] Tang C, Wang JM, Wen GW, Wang Y, Li DY. Bauschinger effect in wear of Cu-40Zn alloy and its variations with the wear condition. *Wear* 2011; 271(9): 1237-1243.
- [20] Xiaoyu H, Chao W, Margolin H, Nourbakhsh S. The Bauschinger effect and the stresses in a strained single crystal. *Scr. Metall. Mater.* 1992; 27: 865-870.
- [21] Gao Y, Wang H, Zhao J, Sun C, Wang F. Anisotropic and temperature effects on mechanical properties of copper nanowires under tensile loading. *Computational Materials Science* 2011; 50: 3032-3037.
- [22] Sainath G, Choudhary BK. Orientation dependent deformation behaviour of bcc iron nanowires. *Computational Materials Science* 2016; 111: 406-415.
- [23] Lieber CM. Nanoscale science and technology: building a big future from small things *MRS Bull.* 2003; 28: 486-491.
- [24] Mughrabi H. Dislocation wall and cell structures and long-range internal stresses in deformed metal crystals. *Acta Metall.* 1983; 31: 1367-1379.
- [25] Liu X, Yuan F, Zhu Y, Wu X. Extraordinary Bauschinger effect in gradient structured copper. *Scr. Mater.* 2018; 150: 57-60.
- [26] Tsuru T. Origin of tension-compression asymmetry in ultrafine-grained fcc metals. *Phys. Rev. Mater.* 2017; 1: 2-4.
- [27] Park HS, Zimmerman JA. Modeling inelasticity and failure in gold nanowires. *Phys. Rev. B* 2005; 72: 054106.
- [28] Olsson PAT, Melin S, Persson C, Atomistic simulations of tensile and bending properties of single-crystal bcc iron nanobeams. *Phys. Rev. B* 2007; 76: 224112.
- [29] Sainath G, Choudhary BK, Jayakumar T. Molecular dynamics simulation studies on the size dependent tensile deformation and fracture behaviour of body centred cubic iron nanowires. *Comput. Mater. Sci.* 2015; 104: 76-83.
- [30] Zhou M, Liang W. Response of copper nanowires in dynamic tensile deformation. *Proc. Inst. Mech. Eng. Part C J. Mech. Eng. Sci.* 2004; 218(6): 599-606.
- [31] Park HS, Gall K, Zimmerman JA. Deformation of FCC nanowires by twinning and slip. *J. Mech. Phys. Solids* 2006; 54: 1862-1881.
- [32] Xie H, Yin F, Yu T, Lu G, Zhang Y. A new strain-rate-induced deformation mechanism of Cu nanowire: Transition from dislocation nucleation to phase transformation. *Acta Mater.* 2015; 85: 191-198.
- [33] Norskov JK. Covalent effects in the effective-medium theory of chemical binding: Hydrogen heats of solution in the 3d metals. *Phys. Rev. B* 1982; 26: 2875.
- [34] Cleri F, Rosato V. Tight-binding potentials for transition metals and alloys. *Phys. Rev. B* 1993; 48: 22.

- [35] Finnis MW, Sinclair JE. A Simple Empirical N- body Potential for Transition Metals. *Philos. Mag. A-Phys. Condens. Matter Struct. Defect Mech. Prop.* 1984; 50: 45.
- [36] Daw MS, Baskes M. Embedded-atom method: Derivation and application to impurities, surfaces, and other defects in metals. *Phys. Rev. B* 1984; 29: 6443.
- [37] Nam HS, Hwang NM, Yu BD, Yoon JK. Formation of an Icosahedral Structure during the Freezing of Gold Nanoclusters: Surface-Induced Mechanism. *Phys. Rev. Lett.* 2002; 89: 275502.
- [38] Cagin T, Dereli G, Uludogan M, Tomak M. Thermal and mechanical properties of some fcc transition metals. *Phys. Rev. B* 1999; 59: 3468.
- [39] Koh SJA, Lee HP, Lu C, Cheng QH. Molecular dynamics simulation of a solid platinum nanowire under uniaxial tensile strain: Temperature and strain-rate effects. *Phys. Rev. B* 2005; 72: 085414.
- [40] Sturgeon JB, Laird BB. Adjusting the melting point of a model system via Gibbs-Duhem integration: Application to a model of aluminum. *Phys. Rev. B* 2000; 62: 14720.
- [41] <http://lammmps.sandia.gov/>. LAMMPS Molecular Dynamics Simulator (Erişim Tarihi:02.04.2021).
- [42] Stukowski A. Visualization and analysis of atomistic simulation data with OVITO—the Open Visualization Tool. *Modelling and Simulation in Materials Science and Engineering* 2010; 18(1): 015012.
- [43] Kazanc S. The effects on the lattice dynamical properties of the temperature and pressure in random NiPd alloy. *Can. J. Phys.* 2013; 91(10): 833-838.
- [44] Kazanc S, Ozgen S, Adiguzel O. Pressure effects on martensitic transformation under quenching process in a molecular dynamics model of NiAl alloy. *Physica B* 2003; 334(3-4): 375-381.
- [45] Saitoh KI, Liu WK. Molecular dynamics study of surface effect on martensitic cubic-to-tetragonal transformation in Ni-Al alloy. *Computational Materials Science* 2009; 46: 531-544.
- [46] Jacobus K, Sehitoglu H, Balzer M. Effect of stress state on the stress-induced martensitic transformation in polycrystalline Ni-Ti alloy. *Metallurgical and Materials Transactions A* 1996; 27(A): 3066-3073.
- [47] Guellil AM, Adams JB. The application of the analytic embedded atom method to bcc metals and alloys. *J Mater Res* 1992; 7: 639–652.
- [48] Foiles SM, Baskes MI, Daw MS. Embedded-atom-method functions for the fcc metals Cu, Ag, Au, Ni, Pd, Pt, and their alloys. *Phys Rev B* 1986; 33: 7983.
- [49] Setoodeh AR, Attariani H, Khosrownejad, M. Nickel nanowires under uniaxial loads: A molecular dynamics simulation study. *Computational Materials Science* 2008; 44: 378-384.
- [50] Wang P, Chou W, Nie A, Huang Y, Yao H, Wang H. Molecular dynamics simulation on deformation mechanisms in bodycentered-cubic molybdenum nanowires. *J Appl Phys* 2011; 093521:110.
- [51] Zhou J, Shen J, Essa FA, Yu J. Twins and grain boundaries-dominated the reverse Bauschinger effect and tension-compression asymmetry. *Journal of materials research and technology* 2022; 18: 15 -28.
- [52] Wu HA. Molecular dynamics study of the mechanism of metal nanowires at finite temperature. *European Journal of Mechanics A/Solids* 2006; 25: 370-377.
- [53] Setoodeh AR, Attariani H. Nanoscale simulations of Bauschinger effects on a nickel nanowire. *Materials Letters* 2008; 62: 4266–4268.
- [54] Jordon JB, Horstemeyer MF, Solanki K, Xue Y. Damage and stress state influence on the Bauschinger effect in aluminum alloys. *Mechanics of Materials* 2007; 39: 920–931.
- [55] Abel A, Muir H. The Bauschinger effect and discontinuous yielding. *Phil Mag* 1972; 26: 489–504.
- [56] Brown LM. Orowan's explanation of the Bauschinger effect. *Scr Metall* 1977; 11: 127–131.
- [57] Zhu D, Zhang H, Li DY. Influence of Nanotwin Boundary on the Bauschinger's Effect in Cu: A Molecular Dynamics Simulation Study. *Metallurgical and Materials Transactions A* 2013; 44A: 2013-4207-4217.
- [58] Abel A. Historical perspectives and some of the main features of the Bauschinger effect. *Mater. Forum* 1987; 10(1): 11–26.
- [59] Horstemeyer MF. Damage influence on Bauschinger effect of a CAST A356 aluminum alloy. *Scripta Mater.* 1998; 39: 1491–1495.
- [60] Caceres CH, Griffiths JR, Reiner P. Influence of microstructure on the Bauschinger effect in an Al Si–Mg alloy. *Acta Metall.* 1996; 44: 15–23.
- [61] Prinz F, Argon AS. Dislocation cell formation during plastic deformation of copper single crystals. *Phys. Status Solidi A* 1980; 57: 741-753.
- [62] Rzychoń T, Rodak K. Microstructure characterization of deformed copper by XRD line broadening. *Arch. Mater. Sci. Eng.* 2007; 28: 605-608.
- [63] Novak V, Sittner P. Stability of dislocation structure. *Acta Universitatis Carolinae-Math et Phys* 1990; 22: 89–94.
- [64] Sohn SS, Han SY, Shin SY, Bae JH, Lee S. Effect of microstructure and pre-strain on Bauschinger effect in API X70 and X80 line pipe steel. *Met Mater Int* 2013; 19: 423–431.
- [65] Han SY, Sohn SS, Shin SY, Bae JH, Kim HS, Lee S. Effect of microstructure and yield ratio on strain hardening and Bauschinger effect in two API X80 linepipe steels. *Mat Sci Engg A* 2012; 551: 192–199.
- [66] De PS, Kundu A, Chakraborti PC. Effect of prestrain on tensile properties and ratcheting behavior of Ti-stabilised interstitial free steel. *Mat Des* 2013; 87–97